

Refined Bayesian Optimization for Efficient Beam Alignment in Intelligent Indoor Wireless Environments

Parth Ashokbhai Shiroya, Amod Ashtekar, Swarnagowri Shashidhar, Mohammed E. Eltayeb
 Department of Electrical and Electronics Engineering
 California State University, Sacramento
 Emails: {parthshiroya, amodashtekar, sshashidhar, mohammed.eltayeb}@csus.edu

Abstract—Future intelligent indoor wireless environments require fast and reliable beam alignment to sustain high-throughput links under mobility and blockage. Exhaustive beam training achieves optimal performance but is prohibitively costly. In indoor settings, dense scatterers and transceiver hardware imperfections introduce multipath and sidelobe leakage, producing measurable power across multiple angles and reducing the effectiveness of outdoor-oriented alignment algorithms. This paper presents a Refined Bayesian Optimization (R-BO) framework that exploits the inherent structure of mmWave transceiver patterns, where received power gradually increases as the transmit and receive beams converge toward the optimum. R-BO integrates a Gaussian Process (GP) surrogate with a Matérn kernel and an Expected Improvement (EI) acquisition function, followed by a localized refinement around the predicted optimum. The GP hyperparameters are re-optimized online to adapt to irregular variations in the measured angular power field caused by reflections and sidelobe leakage. Experiments across 43 receiver positions in an indoor laboratory demonstrate 97.7% beam-alignment accuracy within $\pm 10^\circ$, less than 0.3 dB average loss, and an 88% reduction in probing overhead compared to exhaustive search. These results establish R-BO as an efficient and adaptive beam-alignment solution for real-time intelligent indoor wireless environments.

Index Terms—Bayesian optimization, Gaussian process, acquisition functions, beam alignment, mmWave, 6G, intelligent wireless environments

I. INTRODUCTION

High-frequency wireless communication, spanning millimeter-wave (mmWave) and sub-terahertz (sub-THz) bands, is a cornerstone of next-generation networks, enabling multi-Gbps throughput and ultra-low latency [1]–[3]. Signals at these frequencies, however, are highly directional and suffer strong attenuation when blocked, especially in indoor NLoS environments with walls, furniture, and human activity [4], [5]. These propagation characteristics demand precise and low-latency beam alignment to maintain reliable high-throughput links.

Beam alignment techniques identify the transmit–receive beam pair that maximizes received power. Exhaustive beam sweeping guarantees optimality but incurs prohibitive overhead that scales quadratically with angular resolution. Hybrid, hierarchical [6]–[9], and compressive sensing (CS)-based methods [10]–[12] reduce this cost but rely on channel sparsity and accurate array calibration, assumptions often invalid in reflective indoor environments. Off-grid angles, hardware impairments,

and near-field propagation at high frequencies further degrade their performance.

Learning-based and optimization-driven beam management schemes have recently been explored for beam alignment. Deep learning models can infer beam directions from auxiliary sensing data [13]–[15] but require large datasets and high computational complexity. In contrast, *Bayesian Optimization (BO)* provides a lightweight, model-agnostic alternative that treats received power as a black-box function and efficiently balances exploration and exploitation to locate near-optimal beams using minimal measurements [16].

This paper presents a **Refined Bayesian Optimization (R-BO)** framework for efficient beam alignment in intelligent indoor wireless environments. R-BO leverages the structured spatial power distribution of directional antennas, where received power varies smoothly across adjacent beams, to accelerate convergence toward the optimal beam pair. The framework integrates a Gaussian Process (GP) surrogate with a Matérn kernel and an Expected Improvement (EI) acquisition function, followed by a localized refinement search around the predicted optimum. The GP hyperparameters are adaptively re-optimized to capture evolving angular power variations, enabling fast and low-overhead beam alignment without relying on channel sparsity or array calibration priors. **Contributions:** We develop **R-BO**, a Bayesian optimization framework that combines uncertainty-driven exploration with localized refinement to achieve near-optimal alignment using minimal probes. An adaptive Matérn kernel is employed to track non-stationary angular power distributions in real time. Experimental validation in indoor environments demonstrates **97.7% alignment accuracy**, **88% fewer probes** than exhaustive search, and under **50%** of the probes required by CS-based methods.

II. SYSTEM MODEL

We consider a mmWave beamforming system operating in an indoor environment with a line-of-sight (LoS) path. The transmitter (TX) and receiver (RX) are equipped with t and r antennas, respectively, and employ predefined beamforming codebooks $\mathbf{F} = \{\mathbf{f}_1, \mathbf{f}_2, \dots, \mathbf{f}_p\}$ and $\mathbf{W} = \{\mathbf{w}_1, \mathbf{w}_2, \dots, \mathbf{w}_q\}$, where $\mathbf{f}_i \in \mathbb{C}^{t \times 1}$ and $\mathbf{w}_j \in \mathbb{C}^{r \times 1}$ denote the transmit and receive beamforming vectors, respectively. Following the standard narrowband mmWave MIMO channel model in [8],

the received signal corresponding to a given beam pair $(\mathbf{f}_i, \mathbf{w}_j)$ is expressed as

$$y = \mathbf{w}_j^H \mathbf{H} \mathbf{f}_i s + e, \quad (1)$$

where $\mathbf{H} \in \mathbb{C}^{r \times t}$ represents the channel matrix, s is the transmitted symbol with $\mathbb{E}[|s|^2] = 1$, and $e \sim \mathcal{CN}(0, \sigma^2)$ denotes additive white Gaussian noise.

In conventional models, mmWave channels are assumed to be sparse in the angular domain, with a small number of dominant scatterers contributing most of the received energy. In practical indoor environments, near-field propagation, local scattering, and transceiver hardware imperfections can cause deviations between the measured and ideal array responses, thereby violating the sparsity assumptions commonly used in mmWave channel models. As a result, received power may spread across multiple directions rather than being concentrated in a few strong angle-of-departure (AoD) and angle-of-arrival (AoA) pairs. Efficient beam alignment, therefore, requires identifying the dominant high-power beam directions with minimal measurements.

Let $\mathbf{f}_i \in \mathbf{F}$ and $\mathbf{w}_j \in \mathbf{W}$ denote candidate transmit and receive beams. The received power for a given beam pair (i, j) is defined as

$$P_{i,j} = |\mathbf{w}_j^H \mathbf{H} \mathbf{f}_i|^2. \quad (2)$$

The objective of this work is to identify the optimal transmit–receive beam pair that maximizes $P_{i,j}$ while minimizing the total number of beam probes required.

III. PROPOSED REFINED BAYESIAN OPTIMIZATION FRAMEWORK FOR BEAM ALIGNMENT

The proposed Refined Bayesian Optimization (R-BO) framework formulates beam alignment as a sequential learning problem that exploits the structured angular power distribution inherent in directional transceivers. In indoor environments, strong reflections and hardware non-idealities create received-power fields characterized by multiple lobes, one dominant mainlobe and several weaker sidelobes. As the transmitter and receiver steer their beams, energy from these sidelobes “leaks” into neighboring angles, providing informative gradients that indicate the direction of the true optimum even before it is directly probed. R-BO leverages this angular leakage to efficiently navigate the non-convex angular power landscape and progressively focus the search toward the strongest beam pair with minimal measurements.

Fig. 1 illustrates a representative angle-of-arrival and angle-of-departure relative power map obtained via exhaustive beam search in an indoor environment. In addition to sidelobe leakage, multiple reflected paths generate secondary peaks that make conventional hierarchical and compressive-sensing-based methods inefficient. These secondary peaks depend strongly on user position, proximity to the transmitter, and nearby reflective surfaces, resulting in complex, location-dependent angular power distributions that challenge conventional beam training.

To efficiently identify the dominant beam pair within such complex angular landscapes, R-BO formulates beam alignment

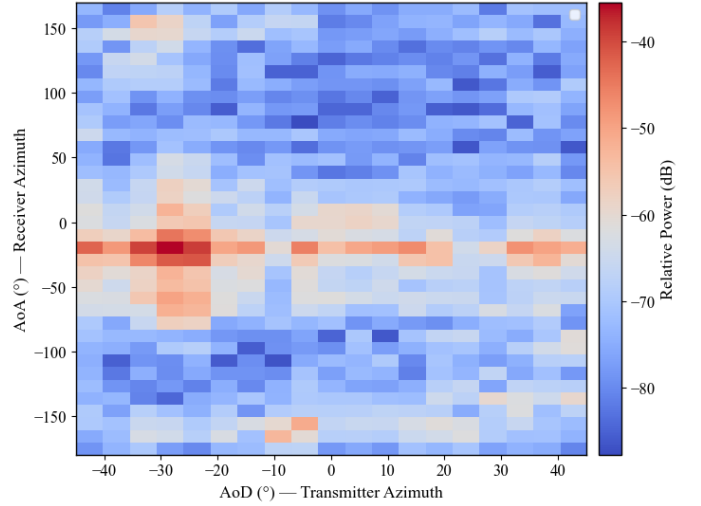


Fig. 1. Measured AoA–AoD relative power map for an indoor environment under exhaustive search. The mainlobe and multiple sidelobes illustrate the non-convex angular power landscape. Measurements were obtained using 16 TX and 16 RX antennas operating at 60 GHz in an indoor laboratory environment at location ID RX23.

as a sequential learning problem. Each beam combination $\mathbf{x} = (\theta_{\text{AoA}}, \phi_{\text{AoD}})$ is treated as a sample of an unknown function $f(\mathbf{x})$ representing the received power. Since evaluating $f(\mathbf{x})$ requires physically steering the transceivers and measuring the response, exhaustive search becomes impractical. Instead, R-BO aims to infer the optimal beam pair \mathbf{x}^* through a minimal number of informative measurements.

The proposed framework achieves this through three stages: (1) initialization, where a small random subset of beams is measured to construct the initial Gaussian Process (GP) prior; (2) iterative Bayesian optimization, which explores and exploits the angular power field using uncertainty-guided sampling; and (3) localized refinement around the predicted optimum to fine-tune the final estimate.

A. Gaussian Process Surrogate

R-BO employs a *Gaussian Process* (GP) surrogate to model the angular power field as a continuous function of beam directions

$$f(\mathbf{x}) \sim \mathcal{GP}(\mu(\mathbf{x}), k(\mathbf{x}, \mathbf{x}')), \quad (3)$$

where $\mu(\mathbf{x})$ is the prior mean (assumed zero) and $k(\mathbf{x}, \mathbf{x}')$ is the covariance function. To preserve angular periodicity, the AoA and AoD values were encoded as sine–cosine pairs before GP regression, ensuring smooth transitions at $\pm 180^\circ$ boundaries. A Matérn kernel captures moderate smoothness between adjacent beams, consistent with the physical continuity of the array radiation pattern and sidelobe structure. After each probe, the GP posterior provides both the mean $\mu_t(\mathbf{x})$ (expected power) and uncertainty $\sigma_t(\mathbf{x})$ for unmeasured beams. The kernel hyperparameters are re-optimized via marginal-likelihood maximization, allowing the model to continuously adapt to variations in the angular power distribution across different regions of the beam space.

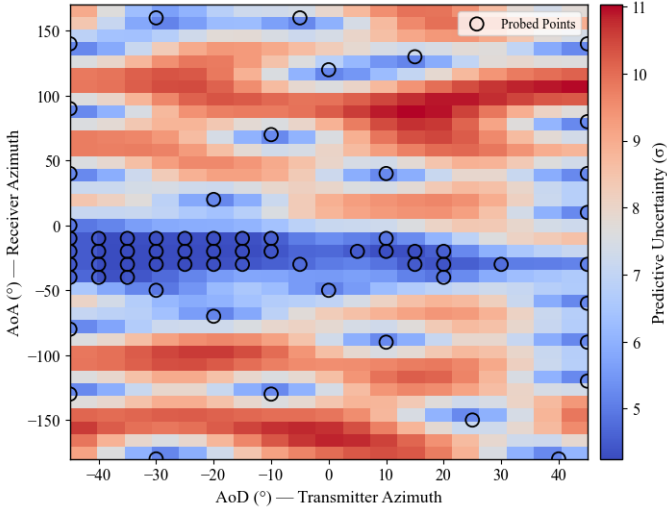


Fig. 2. Posterior predictive uncertainty (σ) map after the Bayesian optimization phase (before refinement). Warmer colors denote regions of higher model uncertainty, while cooler areas indicate well-explored angular regions. Black circles mark the probed beam pairs.

Fig. 2 illustrates the predictive uncertainty (posterior standard deviation) for the same receiver location (RX23) shown in Fig. 1. Unlike the exhaustive relative-power map in Fig. 1, this figure represents the model’s confidence rather than measured power. Unexplored regions exhibit high uncertainty (orange), while well-sampled regions display low uncertainty (blue). The GP thereby provides a principled way to identify beam directions that are most informative for subsequent probing.

B. Acquisition and Sampling Strategy

The next beam pair is selected using the *Expected Improvement (EI)* acquisition function, which balances exploration and exploitation

$$\text{EI}(\mathbf{x}) = (\mu_t - f_t^+ - \xi)\Phi(Z_t) + \sigma_t\phi(Z_t), \quad (4)$$

where $Z_t = (\mu_t - f_t^+ - \xi)/\sigma_t$, f_t^+ is the highest measured power so far, and $\Phi(\cdot)$ and $\phi(\cdot)$ denote the CDF and PDF of the standard normal distribution. The exploration constant, set to $\xi = 0.05$ in this work, encourages broader sampling during early iterations and stronger exploitation as the surrogate converges. By prioritizing beams with high predicted power or large uncertainty, R-BO adaptively concentrates sampling around dominant lobes while discarding weak directions. This adaptive acquisition function drives R-BO to probe only information-rich beam pairs, those with high expected gain or high uncertainty, allowing the GP model to rapidly converge toward the dominant beam direction with minimal sampling. Fig. 3 illustrates this process for RX23, where the red star marks the final beam and the dashed box indicates the local refinement region.

C. Refinement Stage

Once the BO phase identifies the beam pair with the highest posterior mean, a short local probing is performed around that

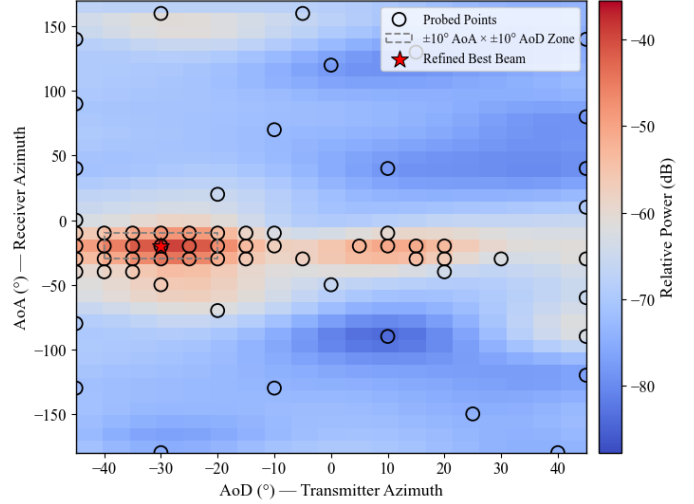


Fig. 3. GP posterior mean (predicted power map) for RX23 after R-BO refinement. The red star marks the final beam; the dashed box shows the $\pm 10^\circ$ local refinement region.

predicted optimum. A $\pm \Delta^\circ$ window centered on the predicted optimum \mathbf{x}^* is scanned to fine-tune the estimate. This step is not an iterative optimization but a one-time local sweep conducted after BO convergence that significantly improves alignment accuracy while incurring negligible additional overhead. The refinement stage does not retrain the GP but performs a direct power scan around the predicted optimum to fine-tune the final selection. The final beam is then selected as the one with the highest measured received power within this local region.

Algorithm 1 summarizes the R-BO procedure. The algorithm alternates between GP model updates and EI-based sampling, followed by localized refinement around the predicted optimum. The GP’s kernel length-scale, signal variance, and noise level were re-optimized via log marginal likelihood maximization at each iteration, ensuring dynamic adaptation to the non-stationary angular landscape observed in indoor channels. All computations in Figs. 2 - 3 were implemented in Python using `scikit-learn`’s `GaussianProcessRegressor` with a Matérn kernel and white-noise term. The following configuration was used: $n_{\text{init}} = 15$ random initialization probes, $T = 50$ Bayesian iterations, and a single $\pm 10^\circ$ refinement stage. The algorithm terminated when the maximum EI across candidates fell below 10^{-8} , indicating convergence.

IV. DATA COLLECTION AND EXPERIMENTAL SETUP

A comprehensive millimeter-wave beam-sweep measurement campaign was conducted in the Wireless Systems Laboratory at California State University, Sacramento, to empirically characterize angle-of-departure and angle-of-arrival power distributions under realistic indoor conditions. Experiments were performed in a closed $12 \text{ m} \times 8 \text{ m}$ laboratory containing metallic benches, computers, and wooden tables that created rich multipath scattering typical of indoor wireless environments. The

Algorithm 1 R-BO for Beam Alignment. \mathbf{X} denotes the matrix of all probed beam coordinates (each row represents one AoA–AoD beam pair, $\mathbf{X} \in \mathbb{R}^{N \times 2}$), and \mathbf{y} is the corresponding vector of measured *received power values*. Each beam pair $\mathbf{x} = [\theta_{\text{AoA}}, \phi_{\text{AoD}}]$ represents one receive–transmit angle combination. A fixed refinement window of $\pm \Delta^\circ$ is applied around the predicted optimum after convergence.

Require: Beam space \mathcal{X} , initial probes n_{init} , iterations T , exploration constant ξ

Ensure: Estimated optimal beam pair $\mathbf{x}_{\text{ref}}^*$

- 1: Randomly select n_{init} beam pairs $\{\mathbf{x}_i\}$ and record the corresponding received powers $\{y_i\}$.
- 2: Assemble the dataset: $\mathbf{X} = [\mathbf{x}_1; \dots; \mathbf{x}_{n_{\text{init}}}]$, $\mathbf{y} = [y_1, \dots, y_{n_{\text{init}}}]^T$.
- 3: Fit a Gaussian Process (GP) with a Matérn kernel to (\mathbf{X}, \mathbf{y}) .
- 4: The GP surrogate models the mapping $f: \mathcal{X} \rightarrow \mathbb{R}$ between beam coordinates and received power.
- 5: **for** $t = 1$ to T **do**
- 6: Compute the posterior mean $\mu_t(\mathbf{x})$ and variance $\sigma_t(\mathbf{x})$ for all unprobed beams.
- 7: Evaluate the Expected Improvement (EI) acquisition and select the next beam pair: $\mathbf{x}_{t+1} = \arg \max_{\mathbf{x}} \text{EI}(\mathbf{x})$.
- 8: Probe \mathbf{x}_{t+1} and record the measured power y_{t+1} .
- 9: **Update:** Append $(\mathbf{x}_{t+1}, y_{t+1})$ to the dataset: $\mathbf{X} \leftarrow [\mathbf{X}; \mathbf{x}_{t+1}]$, $\mathbf{y} \leftarrow [\mathbf{y}; y_{t+1}]$, and refit the GP.
- 10: Re-optimize GP kernel hyperparameters via log marginal-likelihood maximization.
- 11: **end for**
- 12: **Refinement:** Probe all untested beams within a fixed $\pm \Delta^\circ$ window around $\arg \max_{\mathbf{x}} \mu_T(\mathbf{x})$ to fine-tune the final beam estimate.
- 13: **return** $\mathbf{x}_{\text{ref}}^* = \arg \max_{\mathbf{x}} y(\mathbf{x})$

transmitter and receiver were mounted on tripods at a height of 1.6 m to maintain coplanarity and emulate user-equipment (UE)–to–access-point (AP) geometry, as shown in Fig. 4. The floor area was divided into a 7×8 grid of 56 spatial points. The TX was fixed at grid index 53 facing the far wall, while the RX was sequentially placed at the remaining grid locations. A total of 43 RX positions were selected to ensure stable measurements and representative spatial coverage. The setup employed a pair of *Sivers Semiconductors EVK06002* phased-array transceivers operating at 60 GHz in analog beamforming mode. The TX electronically steered beams from -45° to $+45^\circ$ in 5° increments (19 beams), while the RX, mounted on a motorized gimbal, mechanically scanned from -180° to 180° in 10° steps (36 directions). Each RX position therefore produced $19 \times 36 = 684$ AoA–AoD beam-pair measurements. Antenna gains were held constant throughout. Received signal power was measured using an NI USRP-2900 connected to the RX. The LabVIEW interface reports relative power levels in dB; therefore, all reported values in this paper represent relative power rather than absolute power in dBm.

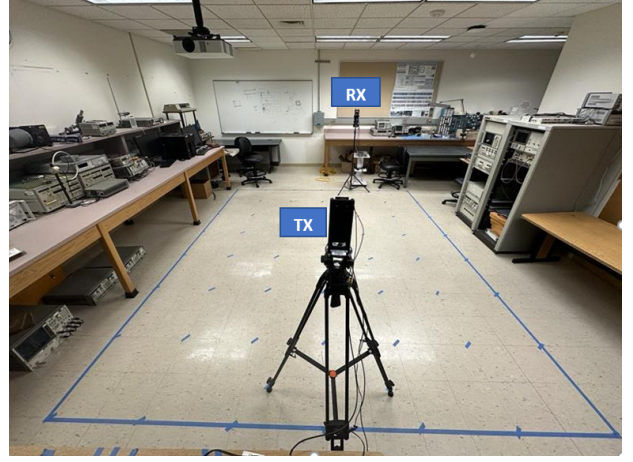


Fig. 4. Room geometry and experimental setup in the Laboratory. The TX was fixed near the center (grid index 53), while the receiver was moved sequentially along marked grid positions to capture spatially distributed beam-sweep data.

V. EXPERIMENTAL RESULTS AND DISCUSSIONS

This section presents the experimental evaluation of the proposed Refined Bayesian Optimization framework using the measured indoor 60 GHz dataset collected in a laboratory environment. All reported results are averaged over 43 receiver positions with direct LoS to the transmitter. The evaluation focuses on alignment accuracy and sampling efficiency, demonstrating that R-BO achieves near-exhaustive beam-search performance with only a fraction of the required probing overhead.

Performance is evaluated using four quantitative metrics: (i) beam-alignment accuracy, defined as the percentage of RX positions where the final beam index selected by R-BO (after refinement) exactly matches the exhaustive-search optimum; (ii) mean absolute error (MAE) of the Gaussian Process (GP) surrogate’s predicted relative power (in dB); (iii) average received-power loss relative to exhaustive beam search (EBS); and (iv) total number of probes per RX. The MAE measures the regression fidelity of the GP model, while the relative power loss quantifies the optimality of the selected beam pair. The refinement radius $\Delta = \pm 10^\circ$ is applied only in the post-optimization refinement stage and is not used as an accuracy tolerance.

Fig. 5 illustrates the convergence behavior of R-BO, showing the average relative power loss as a function of Bayesian iterations for $n_{\text{init}} = 15$. The power loss decreases sharply within the first 20–30 iterations, indicating that the Expected Improvement acquisition function quickly directs exploration toward high-power angular regions. After approximately 50 iterations, the curve stabilizes below 0.3 dB, confirming convergence to the global optimum. This demonstrates R-BO’s ability to efficiently learn the angular power distribution and avoid redundant probing once the dominant region has been identified.

The sensitivity of beam-alignment accuracy to initialization size and iteration count is shown in Fig. 6. The heatmap highlights the trade-off between initial prior information and

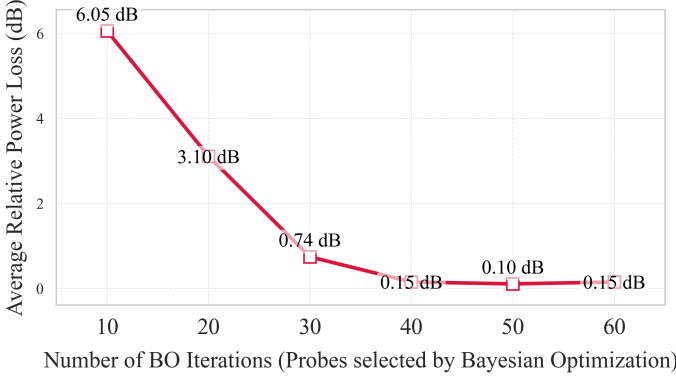


Fig. 5. Average relative power loss versus Bayesian optimization iterations ($n_{\text{init}}=15$) compared to exhaustive search. The loss decreases sharply within the first 30 iterations and stabilizes below 0.3 dB after about 50 iterations, indicating convergence.

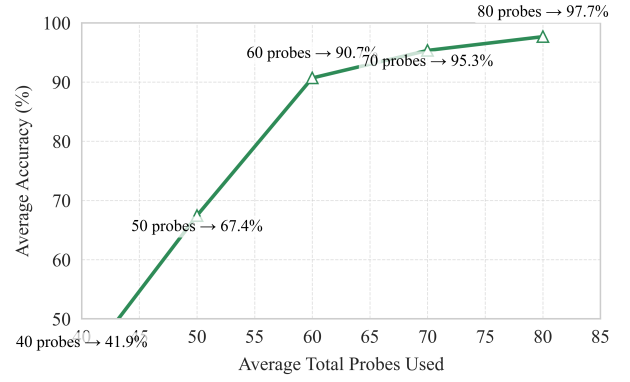


Fig. 7. Trade-off between total probes used and average beam-alignment accuracy. Most accuracy gains occur within the first 60–80 probes, beyond which improvements plateau.

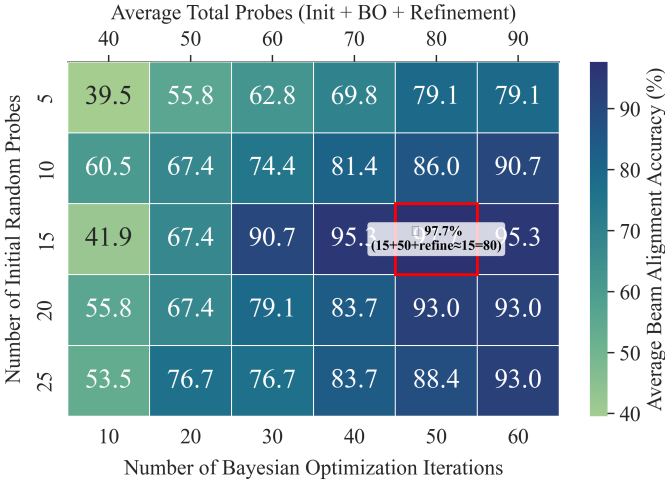


Fig. 6. Beam-alignment accuracy (%) as a function of initialization size and Bayesian iterations. The red cell marks the configuration ($n_{\text{init}}=15$, $T=50$) that achieves the best trade-off between accuracy and sample efficiency.

adaptive exploration. Very small initialization sets ($n_{\text{init}} < 10$) lead to inaccurate GP estimation due to insufficient samples, while excessively large initializations consume unnecessary probes before adaptive focusing begins. Similarly, too few iterations restrict exploration, whereas too many provide diminishing gains. The optimal configuration is found at $(n_{\text{init}}, T) = (15, 50)$, which yields high accuracy with minimal probing overhead and is adopted for subsequent experiments. Although such parameters can be learned from prior environmental data, the proposed framework does not rely on large datasets or data-driven pretraining, unlike deep learning-based approaches.

Fig. 7 shows the trade-off between the total number of beam probes and beam-alignment accuracy. Nearly all accuracy gains occur within the first 60–80 probes, after which improvements plateau. This indicates that R-BO achieves near-optimal accuracy by sampling less than 15% of all beam pairs. In practice, this efficiency enables early termination once a desired accuracy threshold is met, reducing both training latency and energy

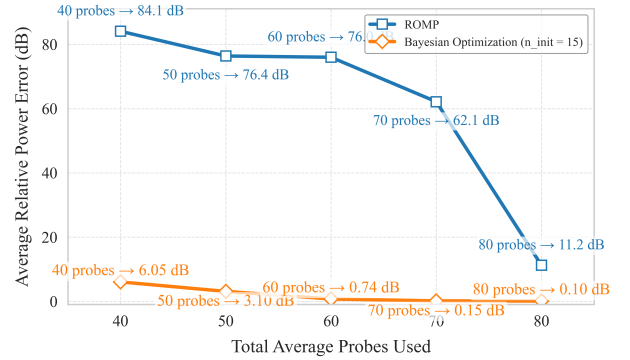


Fig. 8. Average relative beamforming error (dB) versus probe count for Regularized Orthogonal Matching Pursuit (ROMP) and Bayesian Optimization. R-BO achieves faster error reduction and lower steady-state loss.

consumption, an essential advantage for low-power, real-time 6G devices.

R-BO was further compared against a representative compressed-sensing method, Regularized Orthogonal Matching Pursuit (ROMP) [17], as shown in Fig. 8. ROMP assumes sparse angular channels and ideal array calibration, which seldom hold in indoor settings affected by path scattering and hardware imperfections. Consequently, ROMP converges more slowly and suffers higher residual error under reflection and hardware non-idealities. In contrast, R-BO directly exploits measured power feedback without requiring sparsity assumptions or calibration, making it inherently robust to model mismatch. As seen in the figure, R-BO achieves faster error reduction and a lower steady-state loss under the same probe budget. Although ROMP eventually approaches R-BO's performance with a significantly higher number of measurements, this behavior arises because compressed-sensing approaches must reconstruct the entire angular domain, whereas R-BO focuses only on identifying the dominant beams.

A summary of the overall comparison is presented in Fig. 9. Exhaustive beam search achieves perfect alignment by scanning all 684 TX–RX beam pairs per RX but at a prohibitive

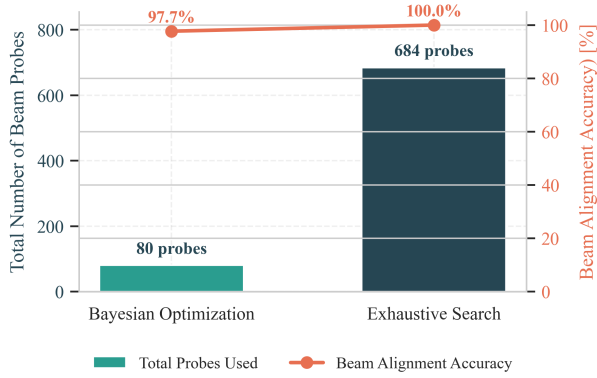


Fig. 9. Average beam-alignment performance comparison between Refined Bayesian Optimization and exhaustive beam search across 43 RX positions. R-BO achieves near-optimal accuracy with an 88% reduction in probing overhead.

computational and measurement cost. In contrast, R-BO attains 97.7% alignment accuracy and less than 0.3 dB average power loss using only 80 probes, corresponding to an 88% reduction in measurement overhead. These results confirm that R-BO’s uncertainty-aware exploration and localized refinement achieve near-exhaustive accuracy with minimal sampling effort, making it an efficient and scalable solution for real-time beam training in intelligent indoor environments.

In summary, R-BO consistently delivers near-exhaustive accuracy with an order-of-magnitude reduction in sampling cost. Its ability to adaptively learn the angular power distribution, exploit sidelobe correlations, and refine locally around the optimum establishes it as a practical and hardware-efficient approach for real-time beam alignment in intelligent indoor wireless systems.

VI. CONCLUSION

This paper presented the Refined Bayesian Optimization framework for efficient beam alignment in high-frequency indoor wireless environments. R-BO integrates Gaussian Process modeling, uncertainty-aware exploration, and localized refinement to identify dominant beam pairs with minimal measurements. Experiments using a measured 60 GHz dataset showed that R-BO achieves 97.7% alignment accuracy and less than 0.3 dB power loss while reducing beam-training overhead by 88% compared to exhaustive search. It also outperforms compressed-sensing-based methods such as Regularized Orthogonal Matching Pursuit, particularly in complex indoor environments where scattering, near-field effects, and hardware imperfections degrade their performance. Future work will extend R-BO to online Bayesian models for dynamic beam tracking and incorporate sensing information such as LiDAR or positioning data to further enhance adaptability across diverse indoor scenarios.

DATA AVAILABILITY

The beam-sweep measurement dataset supporting the findings of this paper has been made publicly available at: <https://github.com/72784/MMWAVE-Dataset>

ACKNOWLEDGMENT

This work was supported by the National Science Foundation under Grant No. NSF-2243089.

REFERENCES

- [1] Q. Xue *et al.*, “A survey of beam management for mmWave and THz communications towards 6G,” *IEEE Commun. Surveys Tuts.*, vol. 26, no. 3, pp. 1520–1559, Third Quarter 2024.
- [2] S. Rangan, T. S. Rappaport, and E. Erkip, “Millimeter wave cellular wireless networks: Potentials and challenges,” *Proc. IEEE*, vol. 102, no. 3, pp. 366–385, Mar. 2014.
- [3] T. S. Rappaport *et al.*, “Wireless communications and applications above 100 GHz: Opportunities and challenges for 6G and beyond,” *IEEE Access*, vol. 7, pp. 78729–78757, 2019.
- [4] O. A. Topal, Z. Li, M. Ozger, D. Schupke, E. Björnson, and C. Cavdar, “Millimeter-wave channel modeling and coverage analysis for indoor dense spaces,” *IEEE Trans. Veh. Technol.*, vol. 74, no. 1, pp. 5–20, Jan. 2024.
- [5] J. Zhang *et al.*, “A survey of mmWave-based human sensing: Technology, platforms and applications,” *IEEE Commun. Surveys Tuts.*, vol. 25, no. 4, pp. 2052–2087, Q4 2023.
- [6] J. Wang *et al.*, “Beam codebook based beamforming protocol for multi-Gbps millimeter-wave WPAN systems,” *IEEE J. Sel. Areas Commun.*, vol. 27, no. 8, pp. 1390–1399, Oct. 2009.
- [7] IEEE, “IEEE802.11-10/0433r2, PHY/MAC complete proposal specification (TGad D0.1),” 2010.
- [8] A. Alkhateeb, O. El Ayach, G. Leus, and R. W. Heath, “Channel estimation and hybrid precoding for millimeter wave cellular systems,” *IEEE J. Sel. Topics Signal Process.*, vol. 8, no. 5, pp. 831–846, Oct. 2014.
- [9] M. E. Eltayeb, A. Alkhateeb, R. W. Heath, and T. Y. Al-Naffouri, “Opportunistic beam training with hybrid analog/digital codebooks for mmWave systems,” in *Proc. IEEE GlobalSIP*, pp. 315–319, 2015.
- [10] M. E. Eltayeb, T. Y. Al-Naffouri, and H. R. Bahrami, “Compressive sensing for feedback reduction in MIMO broadcast channels,” *IEEE Trans. Commun.*, vol. 62, no. 9, pp. 3209–3222, Sep. 2014.
- [11] D. E. Berraki, S. M. D. Armour, and A. R. Nix, “Application of compressive sensing in sparse spatial channel recovery for beamforming in mmWave outdoor systems,” in *Proc. IEEE WCNC*, pp. 887–892, 2014.
- [12] E. Khordad, I. B. Collings, S. V. Hanly, and G. Caire, “Compressive sensing-based beam alignment schemes for time-varying millimeter-wave channels,” *IEEE Trans. Wireless Commun.*, vol. 22, no. 3, pp. 1604–1617, Mar. 2023.
- [13] S. Jiang, G. Charan, and A. Alkhateeb, “LiDAR aided future beam prediction in real-world millimeter wave V2I communications,” *IEEE Wireless Commun. Lett.*, vol. 12, no. 2, pp. 212–216, Feb. 2023.
- [14] S. Wu, C. Chakrabarti, and A. Alkhateeb, “LiDAR-aided mobile blockage prediction in real-world millimeter wave systems,” in *Proc. IEEE WCNC*, pp. 2631–2636, 2022.
- [15] O. Rinchi, A. Alsharoa, and I. Shatnawi, “Deep-learning-based accurate beamforming prediction using LiDAR-assisted network,” in *Proc. IEEE PIMRC*, pp. 1–5, Sept. 2023.
- [16] S. Yang, B. Liu, Z. Hong, and Z. Zhang, “Bayesian optimization-based beam alignment for mmWave MIMO communication systems,” in *Proc. IEEE 33rd Annu. Int. Symp. Pers., Indoor, Mobile Radio Commun. (PIMRC)*, Kyoto, Japan, 2022, pp. 825–830.
- [17] D. Needell and R. Vershynin, “Signal recovery from incomplete and inaccurate measurements via regularized orthogonal matching pursuit,” *IEEE Journal of Selected Topics in Signal Processing*, vol. 4, no. 2, pp. 310–316, Apr. 2010.